Reactions of $C(^3P)$ and $C^+(^2P)$ with NH_3 Studied Spectroscopically at Hyperthermal Energies†

Christoph Ottinger*

Max-Planck-Institut für Strömungsforschung, Bunsenstrasse 10, D 37073 Göttingen, Germany

Andrzej Kowalski

Institute of Experimental Physics, University of Gdansk, ul. Wita Stwosza 57, PL-80−952 Gdansk, Poland

Received: December 20, 2001; In Final Form: May 2, 2002

Chemiluminescent reactions of $C(^3P)$ atoms and $C^+(^2P)$ ions with NH_3 were investigated in the 12−1000 eV_{Lab} (7−586 eV_{CM}) energy range, using a beam/gas arrangement. The fast carbon atoms were generated from $C^+(^2P)$ ions by near-resonant charge transfer with CCl_4. The reaction products NH(A $^3\Pi$), CN(B $^2\Sigma^+$), and CH(A $^2\Delta$) were studied by means of the NH(A−X), CN(B−X), and CH(A−X) emission spectra at 1.4 and 0.35 nm fwhm resolution. Besides, traces of NH(c$^1\Pi$ − a $^1\Delta$), CH(B $^2\Sigma^-$ − X $^2\Pi$), and Balmer line emission were also observed. The reactions were classified as follows: (a) CH(A) is formed by *exchange reactions*, which are assisted by a *hard-sphere-collision mechanism* at high energies to moderate the kinetic energy; (b) NH(A) and NH(c) originate at low energies from *substitution reactions*, and NH(A) also results from *collisional dissociation* at high energies; (c) CN(B) is formed (only at low energies) via a long-lived $[C-NH_3]^+$ *complex*. Detailed evidence for these assignments came from the observed spectra, which were analyzed by means of a computer simulation, as well as from measurements of the energy-dependent relative cross sections.

1. Introduction

Reactions of carbon atoms with ammonia molecules play an important role in nature. It has been suggested that in the interstellar space they are the first step in the generation of amino acids, the building blocks of proteins and the basis of life.[1] Extraterrestrial amino acids have, in fact, been found in meteorites[2] and in lunar samples.[3] Despite this great interest, experimental studies of gas phase C atom reactions are scarce, no doubt due to the difficulties of generating free carbons atoms, and of product detection. Early work has used nucleogenic, energetic ("hot") C atoms, resulting from the $^{14}N(n,p)^{14}C$ reaction inside a nuclear reactor[4] or from the $^{14}N(p,\alpha)^{11}C$ reaction in samples irradiated by a proton beam.[5] The latter technique avoids the complications due to the products suffering radiation damage, as occurs in a reactor. Product detection was facilitated by the radioactive labeling. The high initial recoil energy of the nucleogenic C atoms (45 keV for ^{14}C and ∼3.0 MeV for ^{11}C under the conditions of ref 5) is a disadvantage of this technique. Reaction then takes place at a poorly defined collision energy as a result of multiple moderating collisions. Further problems are the unspecified spin[5,6] and even charge state[4,6] of the reactant carbon species. Later work has used thermal C atoms extracted from an arc discharge.[1] The carbon vapor, assumed to consist of $C(^1D)$ atoms on energetic grounds, was co-condensed with NH_3 on a cold (77 K) surface. This provided for low-temperature reaction conditions and at the same time for product accumulation. The subsequent analysis was done by gas-chromatographic/mass spectroscopic (GC/MS) analysis. Complex secondary reactions in the condensed phase greatly influenced the product distribution, but this was thought to simulate fortuitously the conditions in space to some extent. Gaseous primary products found were CH_2NH (methyleneamine) and HCN (hydrogen cyanide). In addition, however, a nonvolatile product was observed, which did, in fact, upon hydrolysis yield several amino acids.

In the present work, all the difficulties of the previous studies have been eliminated. Single-collision conditions are guaranteed by using an atomic carbon beam. It is generated from C^+ ions by near-resonant charge transfer with a suitably chosen neutralizing gas. In this way, the spin state of the reactant atoms ($C(^3P)$ or $C(^1D)$) can be selected, excess ions can be removed by an electric field, and, most importantly, the collision energy is well-defined and variable. Furthermore, by simply removing the neutralizing gas, one can switch to the study of C^+ ion−molecule reactions. Product detection is also highly specific owing to the use of spectroscopic techniques to distinguish different species. Moreover, in the (most frequent) case of molecular products, even the rovibrational as well as the electronic state of excitation can be uniquely determined, given sufficient spectral resolution.

The beam energy used was varied between 12 and 1000 eV_{Lab}, corresponding to center-of-mass (CM) collision energies of 7.0 to 586 eV_{CM}. This is the typical range of the so-called "hot-atom reactions", an important extension of the common thermal-energy chemistry (see the review[6]). At the same time the hyperthermal energy is well matched to the chemiluminescence (CL) detection scheme. At the elevated collision energies used at least one, but usually several product species were found to emit in the visible or the ultraviolet (Vis/UV). It is, however, possible and even likely that the majority of products originates in their electronic ground state, and thus escapes detection.

† Part of the special issue "Donald Setser Festschrift".

* To whom correspondence should be addressed. Fax:+49 (551) 5176-607.

10.1021/jp014635b CCC: $22.00
Published on Web 07/12/2002

Earlier publications from this laboratory have reported on the luminescent collisions of energetic atoms with simple molecules, i.e., $C + H_2$,[7] $N + H_2$,[8] $N + CH_4$.[9] More details of the apparatus can be found in these publications.

In the course of the experiments, it turned out that the ionic collisions, $C^+ + NH_3$, produced richer emission spectra than the $C + NH_3$ reaction. There exists also a much wider literature on the ionic reaction $C^+ + NH_3$. Under the extreme low-temperature conditions in outer space ion−molecule reactions are generally thought to be more important than neutral/neutral reactions because typically they have no activation energy. They are considered to be the origin of many of the organic species which have been found in the interstellar space by radio-astronomy. In the laboratory, rate constants for the $C^+ + NH_3$ reaction have been measured by ion-cyclotron-resonance (ICR)[10] and selected-ion flow tube (SIFT)[11,12] methods. The product distribution was obtained several times from mass spectrometry,[10−12] but with conflicting results. In all studies NH_3^+ (from simple charge transfer) was found to be a major and HCN^+ a minor product, but disagreement existed as to the importance of H_2CN^+. This ion is assumed to produce HCN molecules in the interstellar space by dissociative recombination with free electrons. Its abundance is therefore critical for modeling the [HCN]/[NH_3] concentration ratio observed in space, which is about 0.4.[13]

A second astrophysical problem which has been studied quantitatively in connection with the $C^+ + NH_3$ reaction is the correct modeling of the [HNC]/[HCN] ratio found in space. The observations on cold dense clouds have yielded values greater than unity, a puzzling result, because HNC is less stable than HCN by 0.64 eV.[14] Despite large-scale ab initio computations[15−18] this problem has not been completely solved.

A noteworthy result of the ab initio calculations[18] was the existence of a potential energy minimum at −4.77 eV below the $C^+ + NH_3$ level which corresponded to a bound complex of $[C-NH_3]^+$ configuration. (Interestingly, for the neutral $C(^1D) + NH_3$ reactions, intermediate bound complexes have also been postulated,[4,5] but ab initio calculations did not show an energy minimum for $[C-NH_3]$[19]). Other, even more firmly bound stable ions having the configurations $HCNH_2^+$ and H_2CNH^+ have experimentally been produced from suitably chosen precursor substances.[20] Their structure was determined by collisional activation (CA) MS, and their binding energy was obtained from high-resolution (50 meV) electron beam appearance energy (AE) measurements. The results were, relative to $E = 0$ for $C^+ + NH_3$, −7.16 eV for $HCNH_2^+$ and −7.42 eV for H_2CNH^+ (the reverse order, with a similarly small spacing, had been obtained in earlier ab initio work[17]). Such deep wells in the $C^+ + NH_3$ potential energy surface are likely to be dynamically observable, and in fact in scattering experiments on this system done at ∼2 eV_{CM}[21] the product ions H_2CN^+ and HCN^+ exhibited angular distributions typical of a reaction mechanism involving an intermediate complex.

Although the present experiments were done at even higher collision energies, here, too, clear evidence for an intermediate complex reaction was found in the formation of $CN(B\ ^2\Sigma^+)$ from low-energy ($\leq$20 eV_{CM}) $C^+ + NH_3$ collisions. From the $C + NH_3$ reaction, no excited CN was observed, nor did any of the other products observed in this work ($NH(A\ ^3\Pi)$, $NH(c\ ^1\Pi)$, and $CH(A\ ^2\Delta)$) exhibit the characteristics of formation via a long-lived complex.

2. Experimental Section

The setup used in the present experiment has previously been described in detail.[7] Briefly, it consists of an ion source, a mass spectrometer, a neutralization cell, a reaction cell, and an optical spectrometer with a photon counting system allowing parallel detection in 1024 wavelength channels. C^+ ions were produced from carbon monoxide at an ion source pressure of ∼25 Pa. The source discharge was run at an anode voltage of 100 V and a current of 0.6 A. Ion beams in the energy range 12−1000 eV_{Lab} were obtained with corresponding beam currents of 0.1−15 nA. For the experiments with neutral C projectiles, the C^+ ion beam was converted into a beam of fast atoms using the near-resonant charge-transfer process

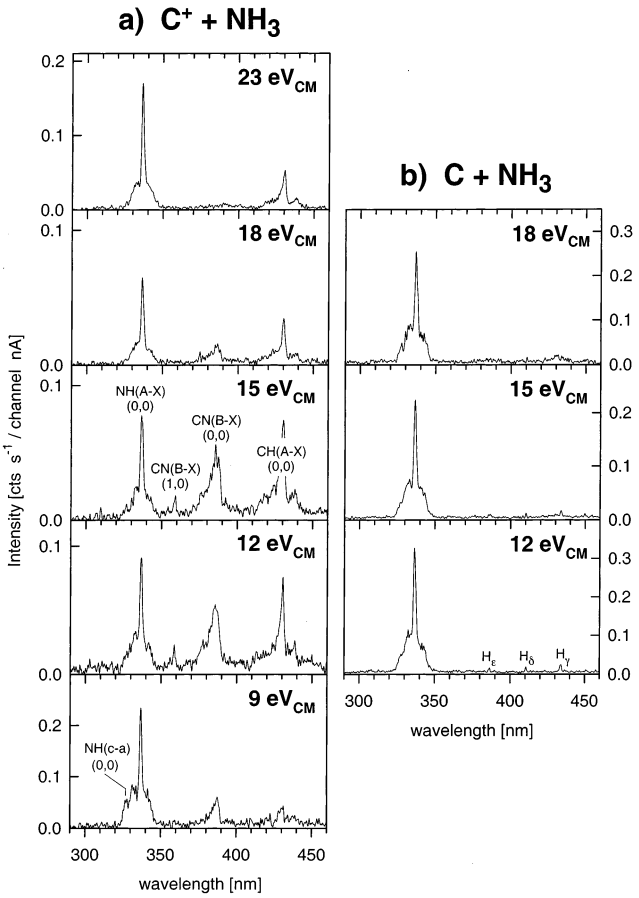

Figure 1. Overview spectra from $C^+ + NH_3$ and $C + NH_3$ collisions at the collision energies indicated. Spectral resolution 1.4 nm. The spectra are smoothed over 7 channels.

$$C^+(^2P) + CCl_4 \rightarrow C(^3P) + CCl_4^+ - 0.214\ eV \qquad (1)$$

Only ground-state $C(^3P)$ atoms should be formed in this way because charge-transfer giving metastable $C(^1D)$ atoms is endothermic by 1.478 eV and is therefore strongly disfavored.

The pressure of the neutralizing gas was on the order of 10 Pa, causing an ion beam attenuation of about 90−95%. The residual ions were prevented from entering the reaction cell by applying a repelling voltage of 200−500 V. However, the ion current measured behind the reaction cell could not be completely suppressed by the electric field. Even at a high repelling voltage, some small ion current (about 1−3% of that observed without neutralization) was measured on a collector plate behind the reaction cell. It resulted most probably from secondary electron emission upon impact of fast atoms on the plate and did not seem to have any effect on the observed chemiluminescence. The spectra were recorded with a multichannel "Mepsicron" detector coupled with a McPherson 218 spectrograph, equipped with a 300 l/mm grating blazed at 500 nm,

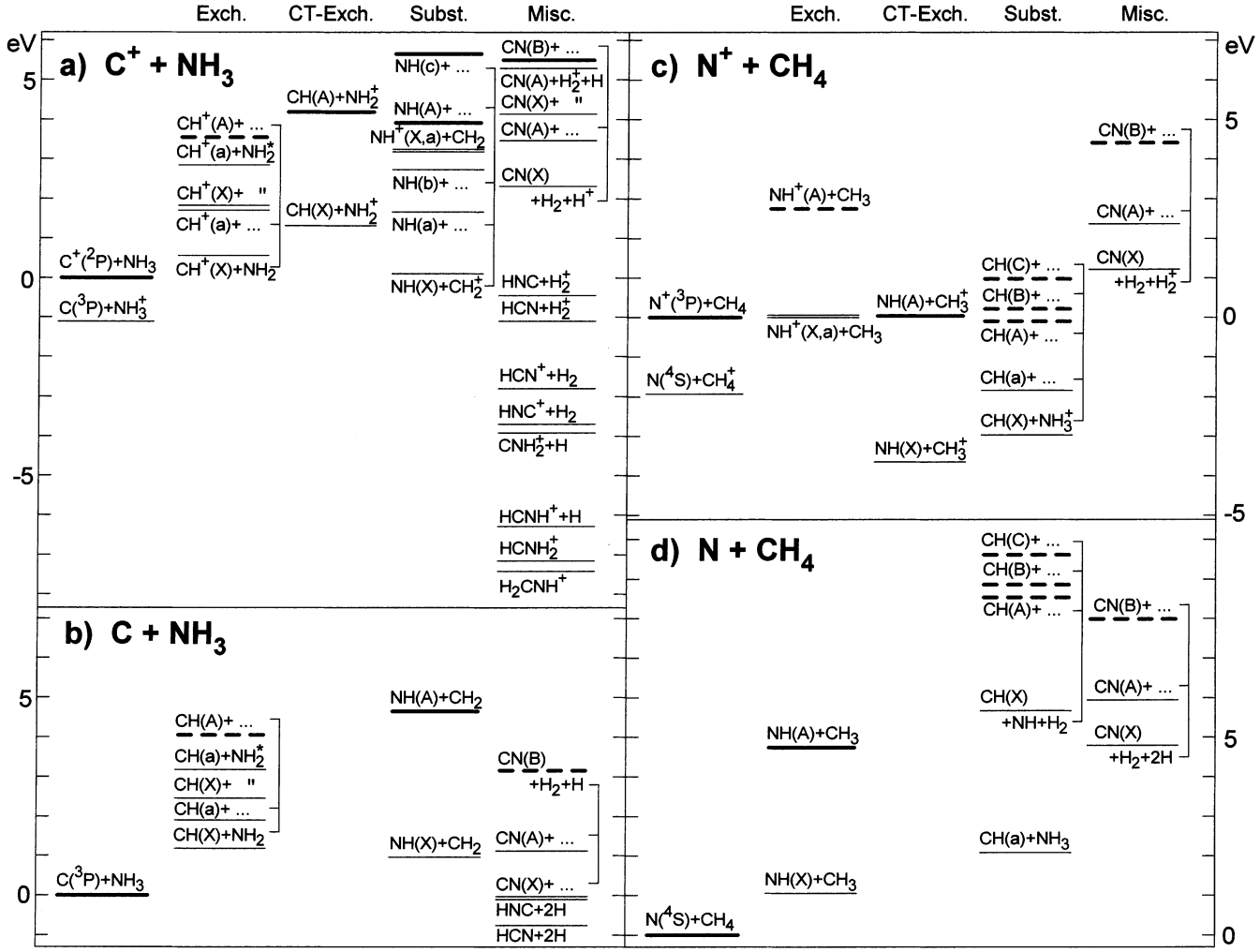

Figure 2. Reactant and product energy levels of the $C^{(+)} + NH_3$ and, for comparison with earlier work,[9,22,23] the $N^{(+)} + CH_4$ systems. Heavy bars: Products observed in emission. Broken bars: levels with possible, but unobserved emission. Thin lines: Unobservable emitter levels. Brackets or ditto marks group together levels with identical "dark" products, for clarity. The levels are organized in columns according to the type of rearrangement involved: Reactants and charge transfer reactants; exchange reaction products; products of charge transfer (CT) with subsequent exchange reactions; substitution reaction; miscellaneous, in particular decay products of an intermediately formed complex.

or, in one case, with a 1200 l/mm grating blazed at 300 nm. Each exposure covered simultaneously a spectral range of 200 nm with a resolution of 1.4 nm fwhm (for the 1200 l/mm grating, a range of 50 nm with a resolution of 0.35 nm). At a target gas pressure of 2 Pa, the NH(A−X), CH(A−X), and CN(B−X) chemiluminescence signals for the $C^+ + NH_3$ reaction, integrated over each band system, were all on the order of 0.8 cts/s at a collision energy of 15 eV_{CM}, whereas the detector dark count rate was 2.7 cts/s.

The experiments were performed in such a way that at each collision energy the CL spectra from the ionic system were recorded first. Thereupon, neutralizing gas was admitted, and the fast atom reaction was studied. Thus, the chemiluminescent intensities of the same molecular product resulting from ionic and neutral reactions could be directly compared. This facilitated greatly measurements of the CL cross sections as a function of the collision energy (for details, see section 3.5).

3. Results and Discussion

3.1 Spectra. Figure 1 gives a survey of the observed spectra, for a selection of collision energies, and for ionic as well as neutral collisions. In total, forty-eight $C^+ + NH_3$ and seventeen $C + NH_3$ spectra were taken between 7 and 586 eV_{CM}, where the range $E_{CM} \leq 60$ eV proved to be the most prolific (only NH(A) emission was observed up to the highest energies, see Figure 6). The spectra show five types of emission features:

(1) Most prominent is the NH(A $^3\Pi$ − X $^3\Sigma^-$) band system around 336 nm. It dominates the spectra at all energies, both for the ionic and the neutral collisions.

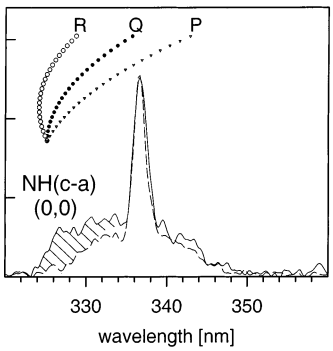

Figure 3. Overlapping NH(c $^1\Pi$ − a $^1\Delta$) and NH(A $^3\Pi$ − X $^3\Sigma^-$) spectra from $C^+ + NH_3$ collisions at 7 eV. Solid contour: Total emission. Dashed: NH(A−X) emission observed at 23 eV (expected to be free from NH(c−a), and to have the identical shape as the—unobservable—"pure" NH(A−X) spectrum at 7 eV would have). Shaded: Difference, ascribed to NH(c−a) emission. The corresponding Fortrat parabolas (up to $J = 22$) are given for comparison. The R branch is known to be exceptionally weak.[33]

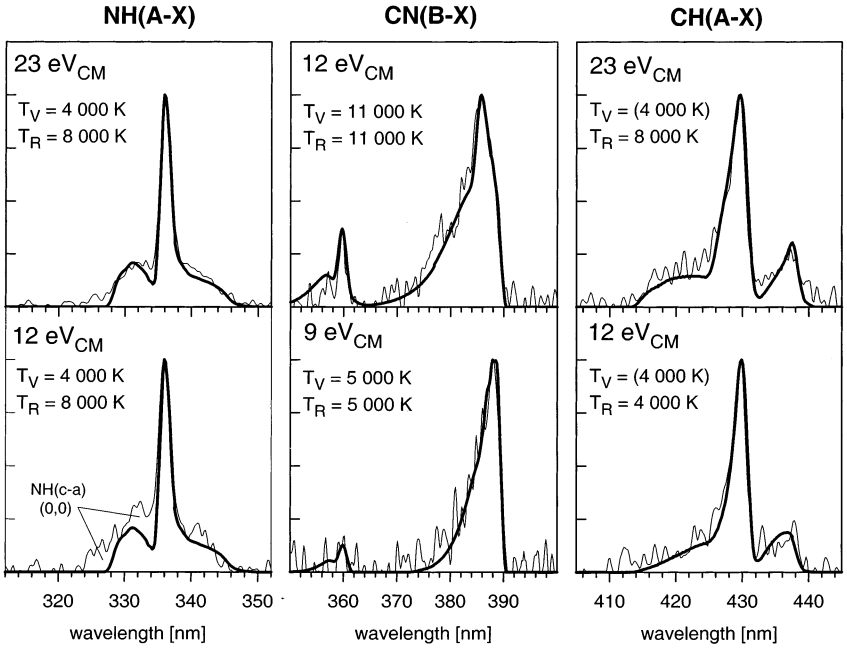

Figure 4. Low-resolution spectra from $C^+ + NH_3$ chemiluminescent reactions at the energies and for the band systems indicated. Thin lines: Observed spectra, from Figure 1 on an expanded wavelength scale and, in the case of CN, after subtraction of some CH(B−X) emission background in the region 388−400 nm. Heavy lines: Simulated spectra, calculated under the assumption of thermal rovibrational level populations in the upper state, with vibrational and rotational "temperatures" T_V and T_R as given.

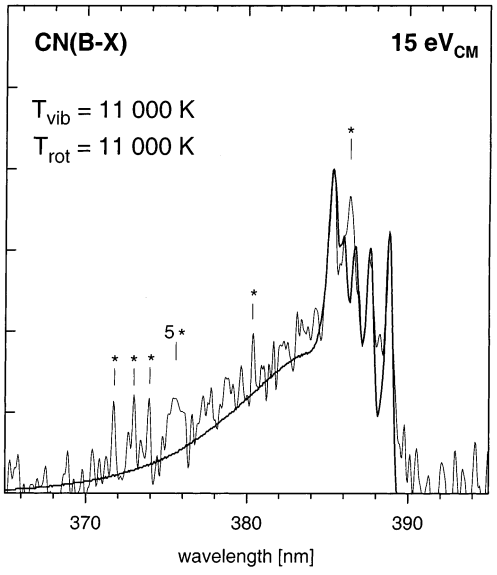

Figure 5. High-resolution chemiluminescence spectrum of the CN-(B−X) $\Delta v = 0$ sequence, from $C^+ + NH_3$ collisions at 15 eV_{CM}. Some carbon line impurities are marked by asterisks and are listed in Table 1. "5*" means a group of five unresolved lines. The three sharp peaks at 388.5, 387.4, and 386.6 nm, and the shoulder at 385.8 nm belong, respectively, to the (0,0), (1,1), (2,2), and (3,3) bands, whereas the 385.3 nm peak is a "head of heads" of many higher $\Delta v = 0$ bands. Observed (thin lines) and computer simulated (heavy lines) contours were matched. The best-fit criteria adopted were: Matching peak height of the (0,0) band at 388.5 nm; good overall fit of the long R-branch from 370 to 385 nm; and, additionally, a good match of the (1,0) band peak at $\lambda \leq 360$ nm from Figure 1. The best-fit parameters T_{vib} and T_{rot} for 15 eV_{CM} are given.

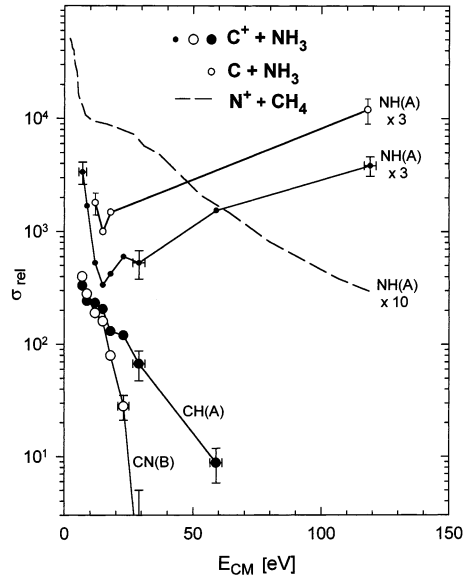

Figure 6. Relative cross sections for generating luminescence from NH(A), CH(A), and CN(B) (solid lines). The corresponding mechanisms are: For NH ≤ 15 eV_{CM}: Substitution reaction; NH ≥ 15 eV_{CM}: Collisional dissociation. For CH ≤ 18 eV: CT-exchange reaction; CH ≥ 18 eV: Hard-sphere collisional energy moderation. For CN: long-lived complex decay. Dashed line: Reference cross sections from,[22] used here for calibration of the ion current energy dependence. It also demonstrates another example of the two reaction mechanisms assumed for CH(A) production, the transition between them being here indicated by an especially well-developed shoulder. For clarity, the NH curves have been displaced upward by factors of three and ten, as marked. The horizontal error bars take into account the energy spread due to the thermal motion of the NH_3 target molecules; the vertical error bars show the statistical uncertainty of the CL signals.

(2) With $C^+ + NH_3$, but not with $C + NH_3$, the CH($A\ ^2\Delta - X\ ^2\Pi$) band system around 430 nm was observed.

(3) Also with $C^+ + NH_3$ only, the CN($B\ ^2\Sigma^+ - X\ ^2\Sigma^+$) emission appeared. Here, two bands are well separated, (0,0) near 388 nm, and (1,0) at 358 nm.

(4) The atomic hydrogen Balmer lines H_γ, H_δ, and H_ϵ were detected as marked in Figure 1b (other spectra further to the red region showed H_β as well).

(5) In Figure 1a at 9 eV, weak NH(c $^1\Pi$ − a $^1\Delta$) emission can be discerned at ~328 nm (better visible in expanded spectra at lower energy, see Figure 3 below).

This rich spectroscopic sample from chemically very different emitters will be interpreted in Sec. 3.3. It is useful, however, to first organize systematically the many potentially contributing reactions according to the types and energetics of the processes concerned.

3.2 Classification of the Observed Processes. Figure 2 shows energy level diagrams of reactants and the most important product combinations. The systems $C^+ + NH_3$ and $C + NH_3$ relevant to this work are shown in panels (a) and (b), respectively. For comparison, energy levels for the reactive systems $N^+ + CH_4$ and $N + CH_4$ studied by us earlier are given in panels (c) and (d) (cf., refs 22,23 and 9, respectively). These systems are largely analogous to $C^{(+)} + NH_3$, and serve as test cases for the interpretations given below. For literature on the energy levels shown in Figure 2, see ref 24.

The layout of Figure 2 is such that observed emitter levels are shown by solid heavy horizontal bars. A priori expected, but unobserved emitter levels are indicated by broken heavy bars, whereas unobservable product levels are given as thin horizontal lines. Only those product combinations were included which are compatible with the overall reactant spin multiplicity, i.e., doublet, triplet, triplet, and quartet in panels a, b, c, and d, respectively.

Purely dissociative processes, i.e., those in which bonds are broken without new ones being formed, are not included. For example

$$C^{(+)} + NH_3 \rightarrow NH(A) + 2H + C^{(+)} \quad (2)$$

has been omitted, but

$$C^{(+)} + NH_3 \rightarrow NH(A) + CH_2{}^{(+)} \quad (3)$$

is included. Dissociative processes occur generally at higher energy. The "dark" products which are complementary to the observed electronically excited species NH*, CN*, CH*, are in general taken to be in their electronically and chemically lowest state, e.g.

$$N + CH_4 \rightarrow NH(A) + CH_3\,(X\,^2A_2'') \quad (4)$$

and not

$$N + CH_4 \rightarrow NH(A) + CH + H_2 \quad (5)$$

An exception is NH_2* in Figure 2a and 2b, which stands for the electronically excited $NH_2(A^2A_1)$ state. Because its emission spectrum in the visible is very broad, it is unobservable in these experiments; the corresponding energy levels are therefore marked by thin lines (a search for $NH_2(A-X)$ emission at $\lambda <$ 600 nm was unsuccessful).

In many instances in Figure 2, three, four, or even five sets of reaction products differ only in the electronic state of the first particle, whereas the "dark" rest is the same. In these cases, to avoid redundancy, the "dark" products are specified only once in each set, and vertical brackets link that level to the others, where the "dark" products are only symbolized by "..." (e.g., in panel (a): $CH^+(X) + NH_2$, $CH^+(a) + ...$, $CH^+(A) + ...$). If only two levels have identical dark products, ditto marks are used instead of brackets for the lower one (as in the same example, $CH^+(a) + NH_2$*, $CH^+(X) +$ ").

The principal types of processes are grouped together in Figure 2 in columns, as follows:

(A) Exchange reaction, the simplest type, labeled "*Exch.*"

Examples: in panel (b)

$$C + NH_3 \rightarrow CH(A) + NH_2 \quad (6)$$

(unobserved) or, for comparison, in panel (d)

$$N + CH_4 \rightarrow NH(A) + CH_3 \quad (7)$$

(observed,[9]).

(B) In the ionic reactions (Figure 2, parts a and c only):

Charge transfer between the reactants prior to the collision proper followed by an exchange reaction, labeled "*CT-Exch.*". Example: in panel (a)

$$C^+ + NH_3 \rightarrow C + NH_3{}^+ \rightarrow CH(A) + NH_2{}^+ \quad (8)$$

(C) Substitution of NH as an entity by $C^{(+)}$, labeled "*Subst.*". Examples:

in (a)

$$C^+ + NH_3 \rightarrow NH(A) + CH_2{}^+ \quad (9)$$

or in (b)

$$C + NH_3 \rightarrow NH(A) + CH_2 \quad (10)$$

Hypothetical substitution reactions for the case of $N^{(+)} + CH_4$ forming CH(A,B,C) at low impact energy are also shown in panels (c) and (d), for completeness. Note, however, that in fact the CH(A,B,C), emission observed in earlier work[23,9] originated not from substitution, but only from simple collisional dissociation of CH_4 (cf., the second half of section 3.3.2).

(D) Miscellaneous processes, in particular those involving CN formation, labeled "*Misc.*". The only observable product is CN(B) (CN(A) emits too far in the red for the detector used). CN(B) was actually detected only in (a), not in (b)−(d). The reason for this will be given below.

3.3 Interpretation. Primarily the following five observations will have to be explained (listed here in the order of the five spectral features highlighted in section 3.1, with which they are associated):

(1) Why is NH(A) emission so prevalent at all energies?

(2) Why is CH(A) not formed from $C + NH_3$ via eq 6 (Figure 1b), in contrast to NH(A) from the closely related $N + CH_4$ reaction eq 7?[9] And why is only CH(A) formed from $C^+ + NH_3$ (Figure 1b) and not CH^+(A), in contrast to the similar $C^+ + H_2$ reaction?

(3) Why is CN(B) formed, a sterically highly improbable product, and why is it only formed in $C^+ + NH_3$ collisions among the four systems shown in Figure 2?

(4) Why do the Balmer lines appear for $C + NH_3$ at collision energies as low as 12 eV_{CM}? This is only marginally sufficient to excite a free H atom into an $n \geq 5$ level, but it certainly does not allow for the dissociation energy of NH_3.

(5) Why is the NH(c) emission so much weaker than that from NH(A), and only visible at all at low energy? The very similar electronic structure of NH(A $^3\Pi$) and NH(c $^1\Pi$) would have suggested comparable intensities.

3.3.1 (We begin with *question 2*). Figure 2d shows that the reaction

$$N + CH_4 \rightarrow NH(A\,^3\Sigma^-) + CH_3 \quad (11)$$

starts on a quartet potential energy surface issuing from the reactants $N(^4S) + CH_4$. This surface correlates adiabatically (not shown) with the quartet surface formed by $NH(X\ ^3\Sigma^-) + CH_3(X\ ^2A_2'')$. The quartet surface formed by the observed product $NH(A\ ^3\Pi) + CH_3(X\ ^2A_2'')$ is the next higher one. Thus, a nonadiabatic transition is required to reach it. This is, however, in principle not a serious impediment, from our experience with many similar chemiluminescent reactions.

In the analogous case of $C(^3P) + NH_3(X\ ^1A_1)$, Figure 2b, the reactants form a triplet surface. The "target" triplet surface connecting with the expected products $CH(A\ ^2\Delta) + NH_2(X\ ^2B_1)$ can here, however, only be reached via a succession of as many as three other, interspersed triplet surfaces: In addition to $CH(X\ ^2\Pi) + NH_2(X\ ^2B_1)$, which connects adiabatically with $C(^3P) + NH_3$, the pairs $CH(a\ ^4\Sigma^-) + NH_2$, $CH(X\ ^2\Pi) + NH_2{}^*(A\ ^2A_1)$, and $CH(a\ ^4\Sigma^-) + NH_2{}^*(A\ ^2A_1)$ all form triplet surfaces (beside some of other multiplicity). Thus, in this case, four successive nonadiabatic jumps are required to yield $CH(A\ ^2\Delta)$ product, the first three offering a competing reaction path. This makes CH(A) effectively inaccessible.

A very similar argument can be put forward to explain the absence of $CH^+(A\ ^1\Pi - X\ ^1\Sigma^+)$ emission, see Figure 2a. However, in addition, there is here another, very strong barrier for this reaction path, which in itself may well be sufficient to suppress $CH^+(A)$ formation. This is suggested by a comparison with Figure 2c. Here, $NH^+(A\ ^2\Sigma^- - X\ ^2\Pi)$ emission is marked as unobserved in $N^+(^3P) + CH_4\ (X\ ^1A_1)$ collisions,[30] although no intervening competing triplet surfaces exist. Apparently the exothermic charge transfer

$$N^+ + CH_4 \rightarrow N + CH_4{}^+ \qquad (12)$$

during the approach phase of this collision is very efficient. $N(^4S) + CH_4{}^+\ (X\ ^2B_1)$ collisions would lead quite naturally to $NH(A) + CH_3{}^+$.

Similarly then, from Figure 2a, the charge transfer

$$C^+ + NH_3 \rightarrow C + NH_3{}^+, \qquad (13)$$

exothermic by 1.11 eV, is expected to be facile, and now only a single nonadiabatic jump is required from the $C(^3P) + NH_3{}^+(X\ ^2A_2'')$ to the $CH(A\ ^2\Delta) + NH_2{}^+(X\ ^3B_1)$ doublet surface. Intense emission from CH(A) is therefore expected, and was in fact observed in the present work. The charge-transfer reaction path is then, according to this view, in strong competition with the path toward $CH^+(A)$, and suppresses the latter.

In our early work on chemiluminescence in the $C^+ + H_2$ system, both $CH^+(A\ ^1\Pi)$ and $CH(A\ ^2\Delta)$ emission were observed side by side.[31,32] The former was, in fact, dominant by far, and CH(A) appeared only at high collision energy. In this case, however, a charge transfer

$$C^+ + H_2 \rightarrow C + H_2{}^+ \qquad (14)$$

is inhibited by the high ionization potential of H_2, I. P.$(H_2) =$ 15.43 eV. With I. P.(C) = 11.26 eV, the charge transfer would be endothermic by 4.17 eV. Question (2) above has thus been answered in both its parts.

3.3.2 Let us now turn to *question (1)* above, i.e., the origin of the great dominance of NH(A) emission, especially at high and at low energies. Particularly the strong NH(A−X) emission at a collision energy as low as 7 eV (see Figure 3 below) lends strong support to the idea that here the NH(A) product originates through the lowest-energy pathways possible, which are the substitution reactions 9 or 10 with threshold energies of 3.9 and 4.7 eV, respectively (Figure 2). The purely dissociative collisions of $C^{(+)}$ with NH_3, eq 2, would be endoergic by 12.5 eV and can be excluded at low energies such as 7 eV.

From Figure 2 it might appear as if the "obstacle race" situation of many competing pathways applied to reaction 9 (although not to 10) and should, therefore, inhibit this reaction.[9] However, this argument is based on potential energy curves along a simple one-dimensional coordinate. For example, in the reaction 6 considered above, this is the usual reaction coordinate, describing the concerted decrease of the C- - -H approach coordinate and the simultaneous increase of the H- - -NH_2 separation coordinate. In the case of reaction 9, by contrast, the reaction coordinate is far more complex. It is here a combination of the decreasing C^+- - -H,H multidimensional approach coordinate with the simultaneously increasing multidimensional H,H- - -NH(A) separation coordinate. Plotting the potential energy surface over these multidimensional geometry parameters will lead to avoided intersections of higher dimensionality, which are expected to be far less restrictive than simple curve crossings at a point in space.

While the substitution mechanism explains the appearance of NH(A) at low kinetic energies, the direct collisional dissociation becomes the dominant mechanism at high energy. Evidence presented below (Figure 6) supports strongly the conclusion that *two* distinct mechanisms contribute to the NH(A) formation in $C^{(+)} + NH_3$ collisions. This answers the question of why NH(A) emission is dominant over such a wide collision energy range (Figure 1). The analogous production of CH(A,B,C) from $N^{(+)} + CH_4$ collisions, on the other hand, *only* proceeds by the high-energy, collisional dissociation mechanism. For the $N + CH_4$ case this is nicely illustrated, in a qualitative way, by juxtaposing Figure 1 of the present work and Figure 1 of ref 9. In the former, NH(A) emission is strong at all energies, while in the latter the corresponding strong CH(A,B,C) emission (especially that from CH(A)) is only observed at high collision energy. Here it is certainly due to straightforward collisional dissociation, as for NH(A) in the present Figure 1. At low energy, however, the CH(A) emission from $N + CH_4$ disappears. The same holds for the $N^+ + CH_4$ reaction, as is shown by the CH(A) cross section curves in Figure 3 of ref 23. Thus the substitution mechanism for $C^{(+)} + NH_3$, eqs 9 and 10, has *no* counterpart in the $N^{(+)} + CH_4$ cases (heavy *dashed* bars in Figures 2c, d).

Two plausible reasons for this can be put forward. First, with one additional atom compared to $C^+ + NH_3$, the substitution mechanisms in $N^{(+)} + CH_4$

$$N^+ + CH_4 \rightarrow CH(A,B,C) + NH_3{}^+ \qquad (15)$$

and

$$N + CH_4 \rightarrow CH(A,B,C) + NH + H_2 \qquad (16)$$

would require a much higher degree of geometrically coordinated motions of the constituent particles than in $C^{(+)} + NH_3$ (in reaction 16, the simpler product combination CH(A,B,C) + NH_3 instead of CH(A,B,C) + NH + H_2 would violate the conservation of the overall spin of 3/2). Second, the C atom in CH_4 is more shielded against reactant attack than the N atom is in NH_3.

In any case, the complete absence of CH emission observed earlier[22,23,9] from $N^{(+)} + CH_4$ at low collision energy, in contrast to the strong NH emission in the present, closely analogous $C^{(+)} + NH_3$ case, demonstrates clearly that simple collisional

dissociation cannot be the origin of the latter. That type of reaction would occur equally in both systems (as is indeed the case at high energies). The substitution mechanism, on the other hand, is so specific that it may well operate only with $C^{(+)} + NH_3$.

3.3.3 *Question 3* above poses a similarly intriguing problem. The formation of (electronically excited) CN radicals in $C^+ + NH_3$ collisions cannot be explained as a simple abstraction or substitution reaction. It indicates a profound rearrangement of all participating atoms. Among the four systems $C^+ + NH_3$, $C + NH_3$, $N^+ + CH_4$, and $N + CH_4$, only the first one gave observable CN(B) emission. Interestingly, this is also the only one which possesses a long-range attractive force between the reactants. This attraction results from the interaction between the C^+ charge and the NH_3 permanent dipole. Such a force is described by a $\propto r^{-2}$ electrostatic potential, while in the $N^+ + CH_4$ case only a $\propto r^{-4}$ charge-induced dipole and in the two neutral systems weak $\propto r^{-6}$ van der Waals attractions operate (in $C + NH_3$ also a dipole−induced dipole interaction, which is likewise $\propto r^{-6}$). This is a clear hint that the CN originates from an intermediately formed, long-lived ionic complex $[C-NH_3]^+$. Initially, the NH_3 molecules would here be oriented with the N atom pointing toward the incoming C^+ ion.

Several ab initio studies have been made of this complex because of the key role which it may play in generating simple amino acids in the interstellar space. All theoretical results agree that it has the structure $H-C-NH_2^+$, resulting from a rapid intramolecular H atom migration. The structure of the ground state is not $[C\cdots NH_3]^+$. For this reason, in Figure 2 the energy levels of the CN manifold have been plotted as $CN + H_2 + H^+$ and not as $CN + H_3^+$. However, the latter set of products cannot be excluded, and in this case all CN levels shown would have to be shifted downward by the proton affinity of H_2, which is 4.38 eV. The reaction

$$C^+ + NH_3 \rightarrow CN(B) + H_3^+ \qquad (17)$$

would then be endoergic by only 1.1 eV. Therefore this decay channel of the long-lived complex, though sterically improbable, would be thermodynamically favored.

Above it was suggested that the formation of $CH^+(A)$ is suppressed in favor of CH(A) as a result of charge transfer (13) in the approach phase. This is not at variance with the present view of $[C\cdots NH_3]^+$ formation, except that the $\propto r^{-2}$ potential would switch to a weaker $\propto r^{-4}$ attraction at some point, where the NH_3^+-charge/C-induced dipole interaction sets in. The $C^+ + NH_3$ charge transfer has been explicitly considered in a correlation diagram given in ref 18.

Further evidence supporting the complex model will be presented below in Secs. 3.4 and 3.5.

3.3.4 As for *question 4*, the Balmer series is most clearly seen in $C + NH_3$ collisions at 12 eV, Figure 1b. In the $C^+ + NH_3$ spectra, Figure 1a, it is not discernible, but may be buried in the noise. Note the different ordinate scales: comparing the 12 eV spectra, the detection sensitivity was 3 times smaller in Figure 1b than in Figure 1a. Also, surprisingly, the Balmer lines are less intense at 15 eV_{CM} than at 12 eV_{CM}, and at 18 eV_{CM} they seem to be absent. This argues strongly against simple dissociative collision as the origin of the excited H atom fragments. Even more convincing is the energetic argument briefly referred to above: The excitation energies of H(n = 5,6,7) are 13.06, 13.22, and 13.32 eV, respectively. With 4.77 eV for the dissociation energy of $D(NH_2-H)$, 17.83, 17.99, and 18.09 eV would be required for the collisional dissociative excitation reactions

$$C + NH_3 \rightarrow C + NH_2 + H^*(n = 5,6,7). \qquad (18)$$

The observation of Balmer lines at a collision energy as low as 12 eV must therefore be due to a different mechanism. Probably the origin is a reaction

$$C + NH_3 \rightarrow HNC + H + H^* \qquad (19)$$

or

$$C + NH_3 \rightarrow HCN + H + H^*. \qquad (20)$$

Figure 2 shows the energy levels of the related reactions giving HNC or HCN plus two ground state H($n = 1$) atoms. They are slightly exothermic, by ∼0.1 eV and ∼0.8 eV, respectively. Therefore at the nominal collision energy 12 eV_{CM}, the H*($n \geq 5$) levels, lying ∼13 eV above H($n = 1$), are just about accessible (considering the experimental spread of E_{CM}). This observation of the Balmer series is an important indirect confirmation of the much discussed role of HCN in $C + NH_3$ collisions in interstellar space. It is remarkable that (from Figure 1b) the H* lines become weaker at 15 eV_{CM} and are not detectable at 18 eV_{CM}. Possibly H* production then gives way to ionizing $C + NH_3$ collisions, yielding $HCN + H + H^+ + e^-$.

$C^+ + NH_3$ collisions could also give H* atoms. Figure 2 shows energy levels of the $CNH_2^+ + H(n = 1)$ and $HCNH^+ + H(n = 1)$ products, at −3.9 eV and −6.2 eV exothermicity relative to $C^+ + NH_3$. Thus H*($n \geq 5$) atoms could here be formed at E_{CM} 9.1 and 6.8 eV_{CM}, but were not observed in this work.

3.3.5 *Question 5* also relates to dissociative processes. As discussed above, the appearance of NH(A) is ascribed at low energy to the substitution reactions 9 and 10. Quite analogously, NH(c) can be formed by substitution at low collision energies. The NH($c\ ^1\Pi - a\ ^1\Delta$) emission shows up as a weak feature in the 9 eV spectrum of Figure 1a, just to the left of the R branch head of the NH($A\ ^3\Pi - X\ ^3\Sigma^-$) spectrum. At higher collision energy it can still be seen in expanded views of this region (see Figure 4 below), but it disappears beyond 12 eV. This is very surprising, since the emitting energy level lies in fact somewhat *above* the NH(A) level (by ∼1.7 eV), see Figure 2. Moreover, the electron configurations of NH(c) and NH(A) are identical, namely $K(2s\sigma)^2(2p\sigma)(2p\pi)^3$. These two states form the well-known singlet/triplet pair of Π levels deriving from such a configuration.

Figure 3 shows the 320−360 nm region on an expanded wavelength scale, compared to Figure 1. 324−345 nm is the region of the NH(c−a) emission in question, as the corresponding Fortrat parabolas in Figure 3 show. It overlaps the R-branch of the close-by NH($A\ ^3\Pi - X\ ^3\Sigma^-$) band system. Subtracting the latter out is not trivial, since its shape at 7 eV_{CM}, isolated from the NH(c−a) contribution, cannot be experimentally determined. Instead, in Figure 3 the NH(A−X) system as observed at 23 eV is shown (dashed). The justification for making this particular comparison comes from computer simulations of the NH(A−X) system, as described in detail in Section 3.4. The essential result was that the A−X spectral contour is independent of the collision energy within the error limits. In fact, the experimental NH(A−X) spectra observed at 7 and 23 eV do match very well in their P-branches, where contamination by NH(c−a) is not a problem. It is therefore safe

to assume that the NH(A−X) R-branches, too, are essentially the same at 23 eV (as shown dashed) and at 7 eV (not directly observable). Comparing then the 325−335 nm region of the A−X and c−a spectra in Figure 3, it becomes clear that the latter makes a substantial contribution to the overall intensity, and is solely responsible for the emission at $\lambda \leq 326$ nm. Thus, at this low collision energy of 7 eV (only 1.5 eV above the calculated threshold energy of NH(c) formation, cf. Figure 2), the NH(c−a) and NH(A−X) emission intensities are indeed of the same order of magnitude, as would have been expected. The fact that the former one is somewhat weaker is largely due to predissociation, which affects the c state much more than the A state, especially in the $v = 1$ level.[34]

At collision energies greater than ~12 eV_{CM}, however, the experiments show clearly that the NH(c−a) emission disappears. This is the regime where we ascribe NH(A) no longer to the substitution reaction 9, but to the direct collisional dissociation

$$C^+ + NH_3 \rightarrow C^+ + NH(A\ ^3\Pi) + 2H(1s) \qquad (21)$$

It has a threshold energy of 12.5 eV, and sustains strong A−X emission up to the highest collision energies studied. Note that conservation of the spin demands that two separate hydrogen atoms be released, which together can balance the NH(A) spin of 1, to equalize the total spin of the NH_3 fragments to that of the original NH_3 molecules, which is zero.

NH(c $^1\Pi$), on the other hand, can in principle be formed either by a reaction corresponding to reaction 21

$$C^+ + NH_3 \rightarrow C^+ + NH(c\ ^1\Pi) + 2H(1s) \qquad (22)$$

where in this case the two hydrogen atoms originate with a combined spin of zero, or by

$$C^+ + NH_3 \rightarrow C^+ + NH(c\ ^1\Pi) + H_2(X\ ^1\Sigma_g^+) \qquad (23)$$

(with a threshold energy of 9.7 eV).

On kinematic as well as statistical grounds, the probability for reaction 23 to occur is much smaller than that for reaction 22. Kinematically, it is quite unlikely that the two hydrogen atoms which are knocked off the N atom in the original NH_3 molecule should recombine into an H_2 molecule. Such a recombination would have to be assisted by the presence of a third body, i.e., the NH radical or the $C^{(+)}$ ion (or atom), and would thus have to take place while the H atoms are departing from the scene. At the ≥10 eV collision energies in question, this is a time interval of only a few fs. There is no such restriction in the case of reaction 22. Statistically, too, the formation of two free H atoms instead of an H_2 molecule is highly favored. Within the bounds set by energy and angular momentum conservation, two separate particles have a much larger volume of phase space available to them than does a single particle formed from them.

This leaves reaction 22 as the only realistic origin of any NH(c $^1\Pi$) in the collisional dissociation regime. Compared to reaction 21, however, reaction 22 is again statistically disfavored. Only $^1/_4$ of the pairs of H(1s) atoms will emerge with a combined spin of zero as in reaction 22, whereas three times as many will have a combined spin of 1, as in reaction 21. For this reason, with the additional suppression of NH(c) emission by strong predissociation, the NH(c−a) system was not observed beside the NH(A−X) emission at high collision energies.

3.4 Simulations of Spectral Contours. Further insight into the mechanisms of the different luminescent processes studied in this work can be obtained from spectral analyses. Because line-by-line intensity measurements would require far higher resolution (entailing unacceptably low signal intensities), the observed spectral contours were modeled by a computer simulation.

The following three band system contours were simulated: (a) NH(A $^3\Pi - X^3\Sigma^-$), from C^+ and C collisions with NH_3, (b) CH(A $^2\Delta - X^2\Pi$), from $C^+ + NH_3$ collisions, and (c) CN (B $^2\Sigma^+ - X^2\Sigma^+$), from $C^+ + NH_3$ collisions.

First, reasonable rovibrational level distributions in the electronically excited state were guessed. Using spectroscopic constants, Franck−Condon factors and Hönl-London factors from the literature,[35−38] the resulting band system contour was then calculated by convoluting each line with the apparatus resolution profile. Finally, the calculated and observed contours were compared, and the level population distributions were adjusted by trial and error until a good overall match was achieved. For simplicity, the rotational level population was assumed to be Boltzmann-like with the rotational temperature T_{rot} as the only variable fit parameter. Further it turned out that the vibrational level population P_{vib} could also be assumed as Boltzmann-like, with a single fit parameter, T_{vib}. The accuracy of the best-fit parameters T_{rot} and T_{vib} is estimated as typically ± 1000 K, and sometimes better.

(a) NH(A $^3\Pi$). The results for NH(A) can be summarized as follows. All NH(A−X) profiles observed in this work, at any collision energy and from $C^+ + NH_3$ as well as $C + NH_3$ collisions, were indistinguishable within the experimental error limits. They were best described by assuming $T_{vib} = 4000$ K, corresponding to the relative population P_{vib} of 1.0:0.3:0.1 for the $v' = 0$, 1, and 2 levels. The best-fit T_{rot} was 8000 K for each of the three levels (also at all energies). T_{vib} was mainly derived from the width of the sharp, high peak in the center of the NH(A−X) spectrum. It is composed of the three Q-branches of the (0,0), (1,1), and (2,2) bands which almost, but not quite overlap. It was found that assuming a greater T_{vib} than 4000 K produces an unrealistic "shoulder" at 338−340 nm on the right flank of the (0,0) Q-branch. T_{rot}, on the other hand, determines mostly the total width of the spectrum, including the R- and P-branch "wings" on the Q-branch peak, cf. Figure 1 and especially the dashed spectrum in Figure 3. A value of T_{rot} significantly lower than 8000 K reduces this width considerably, e.g., to a spread from 330 to 342 nm for $T_{rot} = 2000$ K. Choosing T_{rot} too high, e.g., 20 000 K, produces pronounced "humps" at the R-branch head (328 nm) as well as at the "red" end of the P-branch at ~346 nm (which is determined not by a head, but by the maximum J value set by the NH(A) predissociation at $J_{max} \approx 28$.[34,8] Two sample NH spectra and their simulations are shown in Figure 4 at the left for $E_{CM} = 12$ and 23 eV. It is rather surprising that the NH(A) rovibrational energy is independent of the collision energy, in particular below and above $E_{CM} \approx 12$ eV, i.e., in the regions where NH(A) is formed by the substitution reactions 9 and 10 and by dissociation,[2] respectively. This can perhaps be rationalized by remarking that the projectile does here not become a part of the observed product molecule, and is thus to some extent "decoupled" from the NH(A) rotation. Mechanistically, the NH(A) formation through substitution and through dissociation are basically quite similar. In both cases, two hydrogen atoms are detached from the central nitrogen atom. The difference is only that below 12.3 eV the two H atoms cannot be released as free particles, and have to be bound together by the projectile $C^{(+)}$, to form $CH_2^{(+)}$. Above that threshold all three particles $C^{(+)} + 2H$ are energetically free. One may speculate that the NH(A) is already preformed as an entity within the NH_3 molecule during the

approach of the projectile, and that the decision between formation of $CH_2^{(+)}$ vs $C^{(+)} + 2H$ occurs at a later stage. The effect on the NH(A) radical may, therefore, be quite similar below and above the dissociation threshold energy, in agreement with the observation of identical T_{rot} and T_{vib} values at all energies.

The possibility of charge transfer in the entrance channel discussed in Sec. 3.2.1 does not affect the above reasoning. In fact, the charge distribution in the overall system may even fluctuate as the reaction evolves.

(b) CH(A $^2\Delta$). The simulation of the CH(A−X) emission spectrum gave no information on the P_{vib} distribution. The reason is that at the present spectral resolution the bands of the $\Delta v = 0$ sequence coincide so closely that varying the relative weight of the $v' = 0$, 1, and 2 level populations does not change the resultant combined spectral profile (test simulations with different T_{vib} showed this). The rotational distribution of the emitting CH(A) molecules did, however, reflect distinctly on the overall spectral shape. With increasing T_{rot}, the P branch develops a sharp head at ∼437 nm and the R branch a "hump" at ∼420 nm. The best match with the experimental contour was achieved with $T_{rot} = 4000$ K at 12 eV_{CM} and 8000 K at 23 eV_{CM} collision energy, see Figure 4, right-hand panels. A concomitant increase of T_{rot} with E_{CM} is, in fact, quite plausible. Because in the CT-exchange of reaction 8, the projectile becomes part of the observed product CH(A), a fraction of its kinetic energy reappears in the product rotational energy. This is in contrast to the more complex substitution reactions (9), (10) and the collisional dissociation processes (2) (see the previous section), where the projectile is *not* a part of the observed product NH(A).

(c) CN(B $^2\Sigma^+$). The CN(B−X) emission is especially important. Spectroscopically it can be analyzed with the best accuracy of the three systems studied here because apart from the the $\Delta v = 0$ sequence at 370−390 nm, a weaker $\Delta v = 1$ sequence at 360 nm is also observed. This constrains the P_{vib} distribution much better than in the other cases. Furthermore, the R branches extend a long way into the short-wavelength region, allowing a good fit of T_{rot}. Third, the band structure is such that a high-resolution measurement (0.35 nm fwhm) and its simulation gave additional information. The CN emission is also very remarkable from a dynamical point of view. As explained in section 3.3.3, its appearance is very likely related to the formation of a long-lived ionic complex $[C-NH_3]^+$, possibly to be found in interstellar space, and has hence been the object of many ab initio studies. The spectrum simulations give further support to the complex model.

Figure 4, middle panel, shows two examples of the low-resolution spectra from Figure 1 on the expanded wavelength scale, as well as their simulations. Before fitting, a background correction had to be applied here, which affects particularly the important CN(B−X) (0,0) band peak height at ∼388 nm. This background shows up well in the 12 and 15 eV spectra of Figure 1 between 390 and 410 nm, a region which should be free from CN(B−X) as well as CH(A−X) emission. In fact, the intensity here is due to yet another band system, CH(B $^2\Sigma^-$−X $^2\Pi$). It was observed in very pure form in the earlier $C + H_2$ chemiluminescence study (see ref 7, Figure 2, spectrum taken at 5.7 eV_{CM} at the same resolution as used in the present work). The (red-shaded) head at 387.3 nm of the CH(B−X) (0,0) band overlaps the (blue-shaded) head at 388.5 nm of the CN(B−X) (0,0) band and has to be corrected for. This was accomplished by first matching the CH(B−X) band profile taken from[7] to the "background" emission in Figure 1 in the overlap-free region 390−410 nm, and then subtracting the *entire* CH(B−X) band, from its 387.3 nm head on out to 410 nm, from the recorded intensity profile. This reduces the intensity at $\lambda > 390$ nm down to zero (compare Figure 4 with Figure 1), as it should be, and corrects the right flank of the 388.5 nm peak for the underlying CH(B−X) contribution. The resulting CN(B−X) profile was then fitted by the simulation. To model correctly the spectral contour, it was necessary to include vibrational levels up to $v' = 9$ in the simulation.

TABLE 1: Atomic Lines Observed in the Region of the $\Delta v = 0$ Sequence of CN(B−X) Transition at 15 eV_{CM} Collision Energy (data taken from ref 39)

λ [nm]	element	transition	E_{upp} [eV]	E_{low} [eV]
193.091 (II order)	C I	$3s\ ^1P^o \rightarrow 2p^2\ ^1D$	7.68	1.26
380.431	C I	$7p\ ^1D \rightarrow 3s\ ^1P^o$	10.94	7.68
376.225	C I	$6p\ ^3D \rightarrow 3s\ ^3P^o$	10.78	7.48
375.784	C I	$6p\ ^3D \rightarrow 3s\ ^3P^o$	10.78	7.48
375.705	C I	$6p\ ^3D \rightarrow 3s\ ^3P^o$	10.79	7.49
375.652	C I	$6p\ ^3D \rightarrow 3s\ ^3P^o$	10.78	7.48
375.512	C I	$6p\ ^3D \rightarrow 3s\ ^3P^o$	10.78	7.48
374.079	C I	$6p\ ^3P \rightarrow 3s\ ^3P^o$	10.80	7.48
372.903	C I	$8p\ ^3D \rightarrow 3s\ ^1P^o$	11.01	7.68
∼371.8	C I (?)	unidentified		

The fit results are given in the figure: At 9 eV_{CM}, $T_{vib} = T_{rot} = 5000$ K, and at 12 eV_{CM}, $T_{vib} = T_{rot} = 11\,000$ K. The intensity increase of the $\Delta v = 1$ sequence relative to $\Delta v = 0$ at higher T_{vib} is clearly seen, as is the broadening of the $\Delta v = 0$ peak, which is mainly due to the increased T_{rot}. Figure 5 gives a third CN(B−X) spectrum for 15 eV_{CM}, taken at the higher resolution of 0.35 nm fwhm. This spectrum is somewhat contaminated with atomic carbon lines, which are listed in Table 1. Fortunately, they do not interfere with the CN band simulation. At ∼376 nm there are five such lines in a close group which even shows up in Figure 4. The atomic line emission is believed to originate from electron capture by the C^+ ions traversing the NH_3 target gas. The upper states of these atomic C transitions are all compatible with the available collision energy (Table 1).

The fit shown in Figure 5 provided the most stringent determination of T_{vib} and T_{rot}. The primary fit criterion was, besides a good match of the band contour falloff toward the blue, the correct rendering of the height of the sharp (0,0) band peak at 388.5 nm relative to the normalization peak at 385.3 nm (which is a composite of several bands). This fit was quite critical. It was optimal for $T_{vib} = T_{rot} = 11\,000$ K, the same values as at 12 eV_{CM}. Choosing $T_{vib} = T_{rot}$ greater/smaller by 1000 K had the effect of decreasing/increasing the relative (0,0) band peak height by as much as 12%. Thus the accuracy of the high-resolution measurements of T_{vib} and T_{rot} is estimated as ±700 K. This takes into account partial compensation effects which occur when T_{vib} and T_{rot} are chosen to be unequal, varying them in the opposite sense.

The most remarkable result of the CN simulations is the fact that at 9, 12, and 15 eV the T_{vib} and T_{rot} values, although significantly energy-dependent, are the same within the estimated error limits. This is as expected for a statistical energy redistribution in the decomposing parent complex, and lends strong support to the assumed reaction mechanism. The increase of T_{vib} and T_{rot} with increasing impact energy is plausible. The leveling-off at 11 000 K between 12 eV_{CM} (Figure 4) and 15 eV_{CM} (Figure 5) may indicate the opening-up of additional reaction channels, which absorb the extra energy.

3.5 Reaction Cross Sections. Important information on the reaction mechanisms can also be obtained from the energy dependence of the cross sections for forming the products NH-

(A $^3\Pi$), CN(B $^2\Sigma^+$) and CH(A $^2\Delta$) in C^+ (and C) + NH_3 collisions. The experimental results are shown in Figure 6. On a logarithmic scale, the relative photon yields of these three products are shown as a function of the CM collision energy. They were obtained as follows. First, the areas under the respective spectra were integrated and normalized to the relative spectral detection sensitivity. They were further normalized to the (strongly energy-dependent) C^+ ion current i_C+ (for C + NH_3, $i_C = i_C+$ was assumed). However, account has to be taken of the fact that the ion current i_C+ as measured on a collection plate located behind the collision chamber its not equal to the effective ion current i_C+ through the observation region located at the center of the collision chamber. The reason is the energy-dependent beam spreading as the ions are decelerated prior to entering the collision cell. The difference between the two quantities is not easy to determine. Recourse was therefore taken (following a procedure described in ref 8 for the N + H_2 → NH + H reaction) to a normalization with respect to the reaction

$$N^+ + CH_4 \rightarrow NH(A) + CH_3^+ \qquad (24)$$

studied earlier.[22,23] In that work, care was taken to allow for this effect. To this end, the N^+ + CH_4 reaction 24 was reinvestigated in the present work. This was necessary as the apparatus had been greatly modified since the original N^+ + CH_4 study.[22,23] Let us call the integral intensities of the three band systems I_{NH}, I_{CN}, and I_{CH} and the integral product intensity of the normalization reaction 24 I_o. Then the "apparent" cross sections I_{NH}/i_{C^+}, I_{CN}/i_{C^+} and I_{CH}/i_{C^+} were converted into "true" cross sections $\sigma_{NH}(E)$, $\sigma_{CN}(E)$, and $\sigma_{CH}(E)$ given by

$$\sigma_{NH}(E) = \sigma_o(E) \cdot (I_{NH}/i_C+)/(I_o/i_N+) \qquad (25)$$

for NH, and correspondingly for the CN and CH emissions. Here, $\sigma_o(E)$ is the true cross section for the reference reaction 24, and i_{N^+} is the ion current recorded during the present remeasurement of reaction 24. Along with the results for NH, CN, and CH, Figure 6 shows (dashed) the reference cross section of eq 24 (replotted from Figure 2 in ref 22; for clarity, the original curve has here been shifted upward by a factor of 10). The curves for $\sigma_{NH}(E)$, $\sigma_{CN}(E)$, and $\sigma_{CH}(E)$ are characteristically different.

(a) CH(A $^2\Delta$). The cross section for the hydride ion exchange reaction

$$C^+ + NH_3 \rightarrow CH(A) + NH_2^+ \qquad (26)$$

(large dots) is similar to the analogous H^- exchange reaction of N^+ with CH_4, eq 24. Both exhibit a steep drop at low impact energy, then level off somewhat, and finally decline gradually toward high collision energy. Both the shoulder at medium energies (~20 eV_{CM}) and the final slow drop are less developed for reaction 26 than for reaction 24, but the trends are similar. In particular, the characteristic "tail" for CH(A) from eq 26 is significant. It extends as far as 60 eV_{CM}, a surprisingly high energy for a simple, direct exchange reaction, and is to be interpreted by the same billiard ball model[40] as was invoked for reaction 24 in refs 22 and 23.

At the same time, a comparison of the cross section curve for CH(A) from reaction 26 (large dots in Figure 6) with the reference cross section for NH(A) from reaction 24[22] (dashed in Figure 6) indicates the limits of the simple model. If the billiard ball mass ratio were the only factor determining the probability of forming the diatomic product at collision energies beyond the "chemical" range, then the plateau and the high-energy tail should be equally well developed for CH(A) and NH(A). This follows from the expression for the fractional loss of kinetic energy of the projectile in a head-on collision with a target at rest

$$\frac{\Delta E}{E_0} = -\frac{4\mu}{M} \qquad (27)$$

where E_0 is the Lab system projectile energy, μ is the reduced mass of the collision partners, and M their total mass. For the collision systems C^+ + N and N^+ + C, μ and M are the same. Therefore, the energy loss at equal Lab system energies (and also, to a good approximation, CM system energies), or, in other words, the energy moderation efficiency, is the same in these two cases. Yet reaction 26 has a less pronounced high-energy portion than reaction 24. In the language of the billiard ball model, high-energy C^+ + N collisions are not as effective in slowing down the projectile to the chemical range[6] to form the product CH as are the N^+ + C collisions with respect to NH formation. There are many conceivable reasons for this: The collisions may not be equally "central"; the requirement of a "sufficient" energy moderation may be different; the number of available H atoms to act as a stabilizing third body in the final recombination step is different in NH_3 and CH_4; and certainly many other differences in physical detail. It is nevertheless gratifying to note that the cross section shoulders in Figure 6 occur at about the same collision energies.

(b) CN (B $^2\Sigma^+$). The cross section curve for CN(B) formation is mainly characterized by its steep drop, by 2 orders of magnitude within a ~25 eV_{CM} interval. This is the typical signature of a reaction proceeding through a long-lived complex, in which the constituent particles interact and rearrange statistically. If the impact energy is too high, then the complex lifetime is too short for an internal rearrangement to form CN(B). Thus, the cross section results and the analysis of the CN spectra (section 3.4) consistently support the idea that the reaction

$$C^+ + NH_3 \rightarrow CN(B) + H_2 + H^+ \qquad (28)$$

proceeds through formation of a $[C-NH_3]^+$ complex.

(c) NH (A $^3\Pi$). The cross section curve for NH(A) production from C^+ + NH_3 is the most structured one (for clarity, it has been shifted upward by a factor of 3). It exhibits an initial drop, then passes through a minimum, and finally rises again, persisting up to the highest collision energies studied. This behavior appears to indicate two distinct contributing mechanisms. The first, dominating up to 12 eV, but becoming less efficient at higher energies, can be identified with the substitution reaction 9 discussed in section 3.2. From Figure 2, it has a threshold energy of 3.7 eV. Beyond this (unobserved) onset, the cross section is expected to drop rapidly, because of the requirement of a concerted replacement of NH by the C^+ projectile in the postulated reaction 9. Such an intricate process will be less likely to occur as the collision energy increases. This explains the initial drop. Then, from 12.5 eV on, the simple collisional dissociation eq 21 becomes possible, which is far less dynamically constrained. Other processes giving NH(A) are conceivable at higher energies, and combined they account for the cross section rise beyond ~15 eV_{CM}, and for the persistence of NH(A) fragment emission up to the highest energies employed.

A few additional data points in Figure 6 show the relative cross section for the NH(A) production from *neutral* collisions C + NH_3. Like the data for the related ionic reactions C^+ + NH_3 yielding NH(A), these points have been shifted upward

by a factor of 3. It is seen that the two curves run parallel to each other. The first data point for $C + NH_3$ indicates, in fact, that for this system too, as for $C^+ + NH_3$, the overall cross section passes through a minimum. Thus, for the $C + NH_3$ reaction, the NH(A) product is formed through the same two mechanisms as it is in the $C^+ + NH_3$ case: A substitution reaction 10 at low energies, and from the 12.5 eV threshold on increasingly by straight collisional dissociation, eq 2. This mechanism then persists up to the highest energies, well beyond the typical "chemical" range.[6] It is plausible that at such high energies the charge state of the projectile has little influence on the energy dependence, although the cross section of the neutral C reaction appears to be greater than that of the C^+ reaction by a factor of 3−3.5 throughout.

Here, one has to bear in mind that the cross section measurements of the former suffer from the fundamental difficulty that the C atom flux was not directly measured, unlike the C^+ ion flux. The assumption that these two fluxes are the same is, however, reasonable. At each energy the pressure of the neutralization gas CCl_4 was adjusted such that the C^+ current was almost completely attenuated (to ∼5% of its full value, and these residual ions were then eliminated by applying the retarding voltage). It is to be expected that with this procedure the effective ion and atom fluxes in the reaction cell are approximately equal, i.e., i_C+ in eq 25 can be replaced by i_C.

Finally, we point out that the NH reference curve in Figure 6 can be used to calibrate the absolute magnitudes of the cross sections measured in this work. The same procedure was applied in ref 9 to refer the $N + CH_4$ chemiluminescence cross section to the corresponding cross section for $N^+ + CH_4$. The result is that the 10^4 mark on the ordinate scale corresponds to 1 Å^2 or to 0.25 Å^2, depending on which of two earlier calibrations is correct.

4. Conclusion

Studying elementary chemical reactions under molecular beam/single collision conditions can reveal many microscopic details of the mechanism. Especially the combination with emission spectroscopy is an elegant means of product detection. At collision energies in the eV range, electronically excited products are formed, whose chemiluminescence spectra provide information on the rovibrational state distributions which is otherwise not obtainable. The present study of the $C^+ + NH_3$ and $C + NH_3$ systems has yielded a wealth of dynamical details from the spectra. All three diatomic species that can be formed from C, N, and H were observed, i.e., NH, CH, and CN. Emission in the NH(A−X), NH(c−a), CH(A−X), and CH(B−X) as well as the CN(B−X) systems was detected.

The five striking observations listed in section 3.3 can be explained as follows:

(1) The dominance of the NH(A) emission at all energies stems from *two* contributing mechanisms: Below ∼12 eV, NH(A) is formed by the substitution reactions 9 and 10. Above 12 eV, dissociation (reaction 2) sets in and persists to the highest energies studied.

(2) CH(A) formation from $C^+ + NH_3$ is facile after an initial charge-transfer giving $C + NH_3^+$, eq 8. At the same time, the charge-transfer suppresses CH^+(A) formation. In the $C + NH_3$ system, the pathway to CH(A) is effectively blocked by many competing reaction channels at lower energy.

(3) CN(B) is only formed from $C^+ + NH_3$ and not from $C + NH_3$, because the $C^+ + NH_3$ charge/dipole long-range attraction induces formation of an intermediate, long-lived complex $[C-NH_3]^+$. Within this complex the profound atomic rearrangement takes place which leads finally, after a statistical break-up of the complex, to the emergence of CN(B).

(4) Balmer line emission occurs well below the threshold energy for NH_3 collisional dissociation plus fragment excitation because HCN or HNC formation shifts the energy balance.

(5) NH(c), formed at low energy from $C^+ + NH_3$, appears with much less intensity than NH(A), although the substitution reaction

$$C^+ + NH_3 \rightarrow NH(c\ ^1\Pi) + CH_2^+ \qquad (29)$$

is spin-allowed like its counterpart 9 forming NH(A $^3\Pi$) + CH_2^+. However, the strong predissociation of NH(c) suppresses much of its emission. Beyond ∼12 eV_{CM} the dissociation mechanism

$$C^+ + NH_3 \rightarrow NH(A,c) + 2H + C^+ \qquad (30)$$

takes over. For NH(c), spin conservation requires the two H atoms to be formed with antiparallel spin in order to match the spin zero of NH(c) (formation of $H_2(X\ ^1\Sigma_g+)$ can be excluded on dynamical grounds). However, the singlet state of H + H has only 1/3 of the statistical weight of the H + H triplet state. Thus, in the collisional dissociation regime, NH(c) is discriminated against NH(A) by a factor of 3. With the additional suppression from predissociation, the NH(c−a) transition then becomes unobservable at higher energies.

The measured energy dependence of the relative cross sections to form NH(A), CH(A) and CN(B) bear out these ideas. NH(A) production (both from $C^+ + NH_3$ and from $C + NH_3$) passes through a minimum as the substitution mechanism yields to the collisional dissociation, and continues toward the highest energies studied, increasing slightly. The CH(A) cross section falls off monotonically, but with a shoulder at ∼20 eV_{CM}, followed by a slower falloff to energies beyond 50 eV_{CM}. This latter feature is explained by a hard-sphere C−N collision, which takes up excess energy and allows the "chemical" exchange reaction to proceed up to unusually high E_{CM}. CN(B) is formed only at low energies, the cross section falling off steeply. This is typical of a reaction via complex formation.

The rovibrational analysis of the observed spectra supports in the case of CN the complex mechanism. Rotational and vibrational level populations were found to be thermal, with $T_{rot} = T_{vib}$, both values increasing with E_{CM}. CH(A) is, plausibly, also formed with increasing T_{rot}. A surprise was, however, the fact that NH(A) is formed with the same rovibrational population at all energies, in the substitution as well as dissociation regimes. This is so far unexplained. Hypothetically, the NH(A) may be already released from the NH_3 molecule as the C^+ or C projectile is still rather far away, whatever the impact energy. This idea should be checked by quantum chemical calculations of the structure which an NH_3 molecule adopts in the vicinity of a C^+ ion or a C atom.

Acknowledgment. A.K. gratefully acknowledges support provided by the Alexander-von-Humboldt Foundation and the KBN Grant No. 5 P03B 116 20.

References and Notes

(1) Shevlin, P. B.; McPherson, D. W.; Melius, P. *J. Am. Chem. Soc.* **1983**, *105*, 488.

(2) Kvenvolden, K.; Lawless, J.; Pering, K.; Peterson, E.; Flores, J.; Ponnamperuna, C.; Kaplan, I. R.; Moore, C. *Nature (London)* **1970**, *228*, 923.

(3) Fox. S. W.; Harada, K.; Hare, P. E. *Space Life Sci.* **1972**, *3*, 425.

(4) Yang, J. Y.; Wolf, A. P. *J. Am. Chem. Soc.* **1960**, *82*, 4488.

(5) Cacace, F.; Wolf, A. P. *J. Am. Chem. Soc*. **1965**, *87*, 5301.
(6) Wolfgang, R. *Prog. Reaction Kinetics* **1965**, *3*, 97.
(7) Ehbrecht, A.; Kowalski, A.; Ottinger, Ch. *Chem. Phys. Lett.* **1998**, *284*, 205.
(8) Ottinger, Ch.; Brozis, M.; Kowalski, A. *Chem. Phys. Lett.* **1999**, *315*, 355.
(9) Ottinger, Ch.; Kowalski, A. *Chem. Phys. Lett.* **2001**, *339*, 53.
(10) Anicich, V. G.; Huntress, W. T., Jr.; Futrell, J. H. *Chem. Phys. Lett.* **1976**, *40*, 233.
(11) Smith, D.; Adams, N. G.; *Chem. Phys. Lett.* **1977**, *47*, 145.
(12) Tichý, M.; Rakshit, A. B.; Lister, D. G.; Twiddy, N. D.; Adams, N. G.; Smith, D. *Int. J. Mass Spectrom. Ion Phys*. **1979**, *29*, 231.
(13) Huntress, W. T., Jr.; Anicich, V. G. *Astrophys. J.* **1976**, *208*, 237.
(14) Murrell, J. N.; Derzi, A. Al. *J. Chem. Soc., Faraday Trans. 2* **1980**, *76*, 319.
(15) Allen, T. L.; Goddard, D. J.; Schaefer, H. F., III *J. Chem. Phys*. **1980**, *73*, 3255.
(16) DeFrees, D. J.; Binkley, J. S.; Frisch, M. J.; McLean, A. D. *J. Chem. Phys*. **1986**, *85*, 5194.
(17) Frisch, M. J.; Raghavachari, K.; Pople, J. A.; Bouma, W. J.; Radom, L. *Chem. Phys*. **1983**, *75*, 323.
(18) Talbi, D.; Herbst, E. *Astron. Astrophys*. **1998**, *333*, 1007.
(19) McPherson, D. W.; McKee, M. L.; Shevlin, P. B. *J. Am. Chem. Soc*. **1983**, *105*, 6493.
(20) Burgers, P. C.; Holmes, J. L.; Terlouw, J. K. *J. Am. Chem. Soc*. **1984**, *106*, 2762.
(21) Curtis, R. A.; Farrar, J. M. *J. Chem. Phys*. **1986**, *84*, 127.
(22) Kusunoki, I.; Ottinger, Ch.; Simonis, J. *Chem. Phys. Lett.* **1976**, *41*, 601.
(23) Kusunoki, I.; Ottinger, Ch. *J. Chem. Phys*. **1979**, *70*, 710.
(24) The energies were taken from the following sources: Dissociation energies and ionization potentials come from 25−29. In particular, this fixes the $HCN + H_2^+$ level at 1.08 eV, relative to $E = 0$ for the reactant level $C^+ + NH_3$. The $HCN^+ + H_2$ level is then obtained from the experimental I. P.(HCN),[26] whereas the isomeric spacings $HCN^{(+)}/HNC^{(+)}$ are from 14. Ref 18 gives recent ab initio values for $CNH_2^+ + H$ and $HCNH^+ + H$, directly relative to $E = 0$. The experimental appearance energy AE of H_2-CNH^+[20] fixes the energy of this particular isomer of the $[C-NH_3]^+$ complex relative to the "well-established"[20] $HCNH^+ + H$ level. Finally, the $HCNH_2^+$ isomer was located from its AE[20] to lie 0.26 eV higher.
(25) *JANAF Thermochemical Tables*, 3rd ed.; Natl. Stand. Ref. Data Ser. (U. S., Natl. Bur. Stand.); U. S. GPO: Washington, DC, 1985.
(26) Radzig, A. A.; Smirnov, B. M. *Reference Data on Atoms, Molecules and Ions*, Springer, Berlin, 1985.
(27) *CRC Handbook of Chemistry and Physics*; Weast, R. C., Ed.; 58th edition, CRC Press: West Palm Beach, 1978.
(28) Huber, K. P.; Herzberg, G. *Molecular Spectra and Molecular Structure. IV. Constants of Diatomic Molecules*, Van Nostrand: New York, 1979.
(29) Hack, W. In *Gmelins Handbook of Inorganic and Organometallic Chemistry*, 8th ed., Nitrogen, Suppl. Vol. B1; Koschel, D., Merlet, P., Ohms-Bredemann, U., Wagner, J., Eds.; Springer: Berlin, 1993; p 14.
(30) Kusunoki, I.; Ottinger, Ch. *J. Chem. Phys*. **1979**, *70*, 699.
(31) Kusunoki, I.; Ottinger, Ch. *J. Chem. Phys*. **1979**, *71*, 4227.
(32) Appell, J.; Brandt, D.; Ottinger, Ch. *Chem. Phys. Lett*. **1975**, *33*, 131.
(33) Pearse, R. W. B.; Gaydon, A. G. *The Identification of Molecular Spectra*; Chapman and Hall: London, 1976.
(34) Smith, Wm. H.; Brzozowski, J.; Erman, *J. Chem. Phys*. **1976**, *64*, 4628.
(35) Brazier, C. R.; Ram, R. S.; Bernath, P. F. *J. Mol. Spectry* **1986**, *120*, 381.
(36) Bernath, P. F.; Brazier, C. R.; Olsen, T.; Hailey, R.; Fernando, W. T. M. L. *J. Mol. Spectry* **1991**, *147*, 16.
(37) Nicholls, R. W. *J. Res. NBS* **1964**, *68A*, 75.
(38) Kovács, I. *Rotational Structure in the Spectra of Diatomic Molecules*; Adam Hilger Ltd: London 1969.
(39) Striganov, A. R.; Sventitskii, N. S. *Tables of Spectral Lines of Neutral and Ionized Atoms*; IFI/Plenum: New York, 1968.
(40) Libby, W. F. *J. Am. Chem. Soc*. **1947**, *69*, 2523.